Mid-depth circulation of the eastern tropical South Pacific and its link to the oxygen minimum zone

Rena Czeschel[1], Lothar Stramma[1], Franziska U. Schwarzkopf[1], Benjamin S. Giese[2], Andreas Funk[1] and Johannes Karstensen[1]

[1] Leibniz-Institut für Meereswissenschaften an der Universität Kiel, IFM-GEOMAR,
Kiel, Germany

[2] Department of Oceanography Texas A&M University, College Station, TX, USA

status: 24.09.2010

Corresponding author address:

Rena Czeschel, Leibniz-Institut für Meereswissenschaften, Düsternbrooker Weg 20
24105 Kiel, Germany. E-mail: rczeschel@ifm-geomar.de

Abstract

There is an incomplete description of the mid-depth circulation and its link to the oxygen minimum zone (OMZ) in the eastern tropical South Pacific. Subsurface currents of the OMZ in the eastern tropical South Pacific are investigated with a focus at 400 m depth, close to the core of the OMZ, using several Acoustic Doppler Current Profiler sections recorded in January and February 2009. Five profiling floats with oxygen sensors were deployed along 85°50’W in February 2009 with a drift depth at 400 m. Their spreading paths are compared with the model flow field from a 1/10° Tropical Pacific model (TROPAC01) and the Simple Ocean Data Assimilation (SODA) model. Overall the mean currents in the eastern tropical South Pacific are weak so that eddy variability influences the flow and ultimately feed oxygen-poor water to the OMZ. The center of the OMZ is a stagnant area so that floats stay much longer in this region and can even reverse direction. In one case of one float deployed at 8°S returned to the same location after 15 month. On the northern side of the OMZ in the equatorial current system, floats move rapidly to the west. Most current bands reported for the near surface layer exist also in the depth range of the OMZ. A schematic circulation flow field for the OMZ core depth is derived which shows the northern part of the South Pacific subtropical gyre south of the OMZ and the complicated zonal equatorial flow field north of the OMZ.

INDEX TERMS: 4532 general circulation, 4231 equatorial oceanography, 4516 eastern boundary currents, 4520 eddies and mesoscale processes.

KEYWORDS: ocean circulation, oxygen minimum zone, profiling floats, tropical Pacific Ocean, SODA model, TROPAC01.

1. Introduction

The surface circulation in the upper 100 to 200 m of the eastern tropical/subtropical South Pacific has been well investigated in the last decades [e.g. *Strub et al.*, 1998; *Kessler*, 2006], however the mid-depth circulation at about 200 to 800 m has not been well described due to a limited number of direct observations. Simple dynamical models of ventilated thermocline ventilation [*Luyten et al.*, 1983] predict that streamlines in the southward limb of the subtropical gyre curve anticyclonically away from the eastern boundary, leaving an unventilated "shadow zone" extending westward from the boundary along the northern (equatorward) edge of the gyre. As a consequence there is sluggish ocean ventilation, which is limited to diffusive processes, lateral as well as vertical, and to the exchange with the eastern boundary and the equatorial current system [*Brandt et al.*, 2010], which in the eastern tropical oceans leads to the formation of low oxygen layers. Regions of the interior ocean that are relatively poor in oxygen are often called oxygen minimum zones (OMZs). No clear boundaries are defined for OMZs, here we use 50 μmol/kg oxygen as boundary for the OMZ. Within the shadow zone in the region off Peru there is an oxygen minimum zone (OMZ) that extends from about 100 to 900 m depth [*Karstensen et al.*, 2008]. Because OMZs might expand with time [*Stramma et al.*, 2008] due to changes in oxygen supply and because OMZs are keys to understanding the present unbalanced nitrogen cycle and the ocean's role in atmospheric greenhouse control [*Paulmier and Ruiz-Pino*, 2009] it is important to understand the present-day circulation in the low oxygen areas.

The flow field in the eastern South Pacific, one of the world's four major eastern boundary current systems, is dominated by the Peru-Chile Current system also called the Humboldt Current System (HCS). The coastal geometry connects regions of coastal and equatorial upwelling in the eastern Pacific Ocean. This connection extends to the subsurface Poleward Undercurrent and the surface Peru-Chile Countercurrent, both are in part fed by the Equatorial Undercurrent. According to a recent modeling study it is still unresolved how much the EUC contributes and where it takes place [*Montes et al.*, 2010]. In the PCCS, as in other eastern boundary current systems, the presence of coastal trapped waves, offshore filaments of cold surface water, the outcropping of the oxygen minimum layer close to the coast during upwelling events and the influence of large-scale currents on the coastal system have been described [*Strub et al.*, 1998]. Since currents are generally weak in the eastern tropical Pacific off the eastern boundary these areas are influenced by eddy-like features [*Chaigneau et al.*, 2008] and extra-tropical Rossby waves [*Dewitte et al.*, 2008].

In the equatorial oceans a complicated set of zonal currents exists which have speeds of up to 0.9 m/s for the Equatorial Undercurrent (EUC) at 95°W in October-November 2003 and are described as major supply paths of oxygen to the OMZ [*Stramma et al.*, 2010]. In the eastern Pacific the equatorial currents weaken (for example the EUC at 85°W in March-April 1993 has a speed of 0.6 m/s [*Stramma et al.*, 2010]), in part because of the presence of the Galapagos Island at the equator [*Eden and Timmermann*, 2004; *Karnauskas et al.*, in press]. The most important and best investigated equatorial currents include the South Equatorial Current (SEC) and the North and South Equatorial Countercurrents (NECC, SECC) at and below the surface and the EUC as well as the Northern and Southern Subsurface Countercurrents (NSCC, SSCC) [*Johnson et al.*, 2002] below about 50 m depth. The upper bounds of the OMZs lie in the density range of Subtropical Cells, which connect the subtropical subduction regions of both hemispheres to the eastern, equatorial upwelling regimes by equatorward thermocline and poleward surface flows, together with lower-latitude eastward currents [*Schott et al.,* 2004].

While there is a comprehensive description of the near surface currents derived from some early measurements [*Wyrtki*, 1967] as well as recent summaries [e.g. *Kessler*, 2006] and studies of coastal currents [*Pizarro et al.*, 2002] the open ocean subsurface currents are by comparison sparsely observed. Basin scale descriptions of the South Pacific Ocean circulation were compiled by *Reid* [1986, 1997] based on estimates of the dynamic topography from hydrographic data in combination with tracer data. These compilations revealed interesting details about the general circulation in the Pacific but left out details on the eastern equatorial Pacific subsurface circulation. More recent studies on the South Pacific circulation are based on hydrographic and tracer data [*Fine et al.,* 2001], inverse calculations [*Tsimplis et al.,* 1998] and analysis of numerical model data [*Penven et al.,* 2005; *Montes et al*., 2010]. At 900 m depth autonomous float tracks show weak currents in the eastern tropical South Pacific [*Davis*, 2005]. A strong equatorial intermediate current system exists at 1000 m within 10° from the equator [*Ascani et al. 2010*].

For the tropical North Atlantic a change in subsurface circulation has been identified as a major player for an expanding OMZ [*Brandt et al.* 2010]. To investigate current related changes of the OMZ in the eastern South Pacific and to better understand the existence, formation and maintenance of the OMZ it is necessary to first determine the mean subsurface circulation pathways near the OMZ core. Here, we investigate the subsurface velocity distribution from several ADCP sections and from the paths of profiling floats drifting at a parking depth of 400 m. The velocity distribution and the float paths are related to the oxygen distribution as recorded in a number of CTD-oxygen sections. The results are compared with the 1/10° Tropical Pacific model (TROPAC01) fields as a high resolution open ocean model and the output from the Simple Ocean Data Assimilation (SODA 2.1.6) model to better understand the weak mean flow field in the OMZ. The aim is to derive a mean velocity field for the 400 m depth layer as the core of the OMZ and to describe changes on the same temporal scale as the 1.5 year float mission. The results are combined with previous descriptions in the literature to derive the subsurface circulation in the eastern tropical South Pacific.

2. The data sets

2.1. Observational data

Shipboard CTD and ADCP sections were carried out on two cruise legs of the *RV Meteor* in early 2009. The first leg (M77/3) started in Guayaquil, Ecuador on 27 December 2008 and after several near shelf sections ended in Callao, Peru on 24 January 2009. ADCP data were recorded starting on 5 January 2009 with short sections off Peru at and south of 12°S. From 27 January 2009 to 18 February 2009 the second cruise leg (M77/4) was carried out in the eastern tropical Pacific off South America from Callao, Peru to Panama City, Panama. A vessel-mounted RDI Ocean Surveyor ADCP (75 kHz, OS75) is permanently fixed to the ship's hull and was used during the two cruise legs. The OS75 instrument was used in narrow-band mode with 50 bins of 16m length and measured velocities were averaged into 10 min intervals.

During the second cruise leg hydrographic measurements were made along 14°S, 6°S and 3°35’S as well as along 85°50’W between 14°S and 2°N with the last CTD and ADCP measurements at 2°N on 14 February 2009. The CTD data were calibrated by bottle data for salinity and oxygen by Winkler titration with an oxygen accuracy of 0.5 μmol/kg. The 85°50’W section was measured in March 1993 [*Tsuchiya and Talley*, 1998] and provides the basic water mass information for the 2009 survey. Ten profiling floats with Aanderaa oxygen sensors were deployed between 2 and 11 February 2009 (Appendix B) along the 85°50’W sections at 10°S, 8°S, 6°S, 4°S and 2°S in pairs of 2 floats, one of each pair with a parking depth at 1000 dbar and one with a parking depth at 400 dbar. Both floats have 10 day surfacing intervals. The floats recorded data until mid-August 2010 giving a record of 1.5 years. The Aanderaa oxygen optodes were calibrated for each optode sensor in comparison with CTD-oxygen-casts recorded closely in time and space at the deployment site, as the floats started their mission with a deep profile by a two-point calibration using maximum saturation at the near-surface and minimum saturation (oxygen concentration < 3.5 µmol/kg at around 350 to 400 m depth) in the oxygen minimum layer. The calibrated dissolved oxygen (DO) concentration was then corrected for salinity and pressure effects using the float pressure and salinity readings [*Aanderaa Manual*] but using a higher pressure correction of 5.5% per 1000 dbar.

2.2. Model data

The output data from two different numerical models, the prognostic TROPAC01 and the assimilation model SODA 2.1.6, is used in this study to better understand the mean flow field in the OMZ. The modeling approaches of both models differ fundamentally in forcing and horizontal resolution described as follows.

2.2.1 The TROPAC01 model

Based on the “Nucleus for European Modelling of the Ocean” (NEMO, v3.1) [*Madec*, 2008], the DRAKKAR cooperation [*Barnier et al.*, 2007] developed a global ocean-sea-ice model whose 1/2° horizontal resolution version (ORCA05) with 46 vertical levels (20 levels in the upper 500 m depth) is utilized to embed the 1/10° high-resolution model of the Topical Pacific (TROPAC01). The implementation of the higher resolution region works via two-way nesting using Adapted Grid refinement in Fortran (AGRIF) [*Debreu et al.,* 2008]. The nested domain spans the tropical/subtropical Pacific from 31°N to 49°S extending from the western coast of America (63°W) throughout the entire Pacific

Ocean, reaching into the Indian Ocean at 73°E. The hindcast experiment analyzed here is forced by a compilation of atmospheric reanalysis products [*Large and Yeager*, 2009] and observational data for 1948 to 2007 as given by the Coordinated Ocean-ice Reference Experiment (CORE v2) [*Griffies et al.,* 2009].

2.2.2 The SODA assimilation model

SODA combines the Los Alamos implementation of the POP (Parallel Ocean Program) model with a sequential estimation data assimilation method [*Carton et al.*, 2000; *Carton and Giese*, 2008]. The SODA version used for this paper (SODA 2.1.6) is similar to the version described by *Carton and Giese* [2008], but with some important differences. For the remainder of the paper we use SODA to mean the SODA 2.1.6 product mapped onto a uniform 0.5°x0.5°x40-level grid (19 vertical levels in the upper 500 m depth). Version 2.1.6 is forced by ERA-40 wind stresses from 1958-2001 and by ERA-interim for the period from 2002-2008. Use of the ERA-interim winds makes a more seamless transition between the two periods, and reduces spurious variations excited at the 2001-2002 boundary. As in earlier versions, SODA 2.1.6 assimilates all available data from hydrographic stations, XBTs, and floats, but does not use satellite altimetry. In this version, hydrographic observations come from WOD09 [*Boyer et al.,* 2009] using their standard level temperature and salinity data. Thus these data have been corrected for the drop-rate error as described by *Levitus et al.* [2009]. Experiments with SODA show that applying the *Levitus et al.* [2009] drop-rate correction reduces much of the decadal variability observed in both the hydrographic observations and in ocean reanalyses [*Giese et al.,* 2010].

3. Oxygen distribution and circulation in the eastern tropical South Pacific

3.1. Circulation at 400 m depth in early 2009

The oxygen minimum zones of the tropical eastern Atlantic and Pacific oceans are described to be located in the shadow zones of the oceans [*Karstensen et al.,* 2008]. As the floats drift at 400 m depth close to the center of the OMZ between 6°S and 10°S in the open ocean, the oxygen and velocity fields are presented at 400 m depth.

From the ADCP velocities at 400 m depth in January/February 2009 (Figure 1a) several of the previously described zonal equatorial intermediate current bands [e.g. *Rowe et al.,* 2000; *Stramma et al.,* 2010] can be identified. North of the equator, the westward North Equatorial Intermediate Current (NEIC) and the Equatorial Intermediate Current (EIC) can hardly be separated into an off (north) and an equatorial branch. South of the equator at about 2°S the South Intermediate Countercurrent (SICC) carries water northeastward. At about 4°S the South Equatorial Intermediate Current (SEIC) is fed in part by the SSCC. The SSCC feeds the Peru-Chile Countercurrent (PCCC), which can be followed southward away from the shelf to the southernmost measurements at 18°S. The PCCC is known to extend from 7°S to 40°S approximately 100-300 km offshore [*Strub et al.,* 1995]. Near the shelf the Peru Coastal Current (PCoastalC) carries water equatorward to the northernmost section at 3°35’S. At the 14°S section at about 79°W to 81°W the Humboldt Current/Peru Chile Current (HC/PCC) splits into a northern and southern branch of the SEC, a westward continuation of the HC/PCC with eddies to the east and to the west. These eddies are present in altimeter data from early February 2009 at this location (Figure 1b). At 12°S eastward flow of the SECC exists at 85°50’W but returns westward with the SEC.

In the climatological mean the center of the OMZ at 400 m depth is located at about 8°S at 85°W (Figure 1a). According to the current distribution at 400 m depth in February 2009 the center of the OMZ is located between the eastward and southward flowing SSCC and PCCC to the north and east and the westward flowing SEC to the south. East of the PCCC near the shelf, oxygen concentration reaches its lowest values. Here the PCoastalC carries cold, salty and low oxygen water north. It is respiration in the regions of enhanced productivity, associated with the upwelling that consumes virtually all oxygen. In the equatorial region the highest oxygen values at 400 m depth are found between 4°S and 2°N supplied by equatorial eastward currents [*Stramma et al.* 2010] while in February 2009 only the SICC was found at 400 m depth.

3.2 Zonal oxygen and velocity distribution along 85°50'W

The oxygen distribution at 85°50'W shows the lowest oxygen values of less than 4 µmol/kg at about 400 m depth between 6°S and 10°S. This region has the largest vertical extent of the OMZ with a layer thickness of about 200 m of low oxygen water (< 4 µmol/kg). In the equatorial region north of 6°S the vertical extent of the OMZ is much smaller and the minimum (< 10 µmol/kg) is not as low as that in the south and is located shallower at 300 to 350 m depth. In the upper 250 m the oxygen is higher north of 6°S (> 30 µmol/kg) representing the region of oxygen supply by the equatorial current bands [*Stramma et al.*, 2010].

All five floats were deployed on a section along 85°50'W in February 2009 and ADCP measurements were also carried out along this section. The ADCP distribution for the upper 700 m between 14°S and 2°N at 85°50'W in February 2009 (Figure 2b) shows a complicated zonal equatorial current system. The core of the EUC is located just north of the equator at 15 to 30 minutes north with eastward velocities of about 10 cm/s. However, a second even stronger subsurface eastward current is located at 1°N to 1°40’N. The northern equatorial branch of the westward flowing SEC(n) is present at 2°N. The southern equatorial branch (SEC(s)), which recirculates water from the SSCC, is located between 2°S and 4°S. Between 5°S and 6°20’S the SSCC flows eastward with cores at 100 to 200 m and 400 to 500 m depth, with currents that reach all the way to the surface. The lower core of the SSCC shows strong velocities of about 20 cm/s. The eastward current at 10°S might be either a second core of the SSCC which exists in the South Pacific, or a part of the SECC centered at 12°S. Eastward velocities up to 10 cm/s can be found between 40 to 260 m. South of 12°30’S the westward flow associated with the HC/PCC, and as a southern branch of the SEC can be found.

At mid-depth the SICC and a weak North Intermediate Countercurrent (NICC) are seen as relative maxima of the eastward flow and are strongest at a depth of around 500 m at about 1.5° north of the equator. *Firing et al.* [1998] describe the westward SEIC as being centered around 500 m. In February 2009 the SEIC was strongest at 4°S with velocities of 10 cm/s. A westward EIC is often found below the EUC in the western Pacific; however, the EIC tends to be very weak or nonexistent in the east [*Johnson et al.*, 2002]. In February 2009 there is westward flow at the equator between 150 and 550 m and hence there is a relatively strong EIC of about 10 cm/s.

It can’t be expected that model runs reproduce instantaneous velocity measurements since the ADCP sections are influenced by eddy variability and wave processes. Nevertheless, it is of interest to explore how well models describe the observed flow field and the later derived mean circulation. Except for one structure at 85°50’W located north of 4°S (Fig. 1b) on 4 February 2009, maps of altimeter derived sea level anomaly do not indicate large sea level anomalies (SLA) at the time the 85°50’W section was occupied (Figure 1b). However, on 11 February when the ADCP measurements were being taken on the northern part of the 85°50’W section the anomaly shifted northward to north of 2°S and might be responsible for an eastward surface flow that is larger than those in the model runs. Due to the low SLA changes the 85°50’W section can be compared to model runs. The coarse model grid spacing is too large to resolve well the small current bands and thus shows primarily the mean flow field. Nevertheless it is worthwhile to compare observations and models to find out which processes the models reproduce. Because model runs include the recorded wind fields, and in case of assimilation models in situ data, they are not representative of the most recent years. The float deployment in February 2009 was at the beginning of an El Niño year (2009 to 2010) and since the model runs do not yet include 2009 we use the year 2002 for comparison because it is also the beginning of an El Niño year (2002 to 2003).

At the equator the 85°48’W section from TROPAC01 in February 2002 shows the EUC and EIC (Figure 2c) similar to the observations, however TROPAC01, as well as SODA, (Figure 2d) show a strong westward flow in the surface layer above the EUC. The SODA section at 86°W for February 2002 reproduces the EUC and the EIC (Figure 2d), although the EUC is 5 times stronger than in the observations. Both models show the SSCC current band at 6°S and 8°S, as well as two SECC current bands south of 10°S, although are located at different locations and have different depth structure compared to the observations. Both models do not resolve the small and weak mid-depth equatorial current bands in February 2002 as they do in most (some) of the other months in TROPAC01 (SODA). Similar to the observations the model results show current bands that extend deep into the ocean south of about 4°S and a complicated and vertically reversing flow field north of about 4°S.

3.3. Meridional oxygen and velocity observations

The oxygen section at 3°35’S (Fig. 3a) shows a shallow oxygen minimum of less than 4 µmol/kg at about 300 m depth which slightly widens close to the South American continent. A different oxygen distribution is found at 6°S (Fig. 3b) where the oxygen minimum (< 4µmol/kg) is at 400 m depth at 85°50’W and the minimum widens and spreads upward to 300 m near the shelf. At 14°S (Fig. 3c) the oxygen minimum (< 4 µmol/kg) is located shallower, at about 250 m depth in the west rising to almost 200 m in the east.

At 3°35’S the meridional velocity distribution (Fig. 3d) shows current bands with low vertical expansion, while at 6°S (Figure 3e) and 14°S (Fig. 3f) most current bands extend vertically over the upper 700 m. The altimeter SLA at 3°35’S in early February 2009 (Figure 1b) does not show such large anomalies. The velocity distribution (Figure 3d) indicates a northward contribution of the SSCC to the SEIC between 84°W and 85°W with cores at 100 to200 m and 300 to400 m depth. In the upper 400 m east of 84°W the southward flowing PCCC has velocities of up to 10 cm/s is the PCCC. Near the continental slope there is the Poleward Undercurrent (PUC) or Peru-Chile Undercurrent typically found at 150 to 200 m depth such as is found at 6°S (Fig. 3e). The PUC originates from the Equatorial Undercurrent and carries low oxygen water southward [*Strub et al.,*, 1998], but extends to 600 to 700 m depth [e.g. *Penven et al.*, 2005] and shows a second core at 300 to 400 m depth at 3°35’S with velocities of about 6 cm/s (Fig.3d). Inshore of the PCCC and near the shelf the northward PCoastalC is described as a surface current, however at 3°35’S the PCoastalC is near the surface at 82°15’W and covers the layer 200 to 400 m depth to the east with velocities of about 8 cm/s connected to a deep northward current core at 400 to 700 m near the shelf.

At 6°S the SLA shows a weak anticyclonic eddy between 84 and 86°W (Fig. 1b) in early February 2009. This feature is clearly present in the observed velocity field (Fig. 3e) with strong near-surface velocities in the northward component and a deep-reaching structure of the southward component including the southward shifting SSCC (Fig. 1). In the upper 200 m the core of the PCCC is centered at 82°45’W and is related to lower oxygen values than west of it. The PUC is located at the eastern end of the section and is related to the low oxygen with dissolved oxygen of less than 10 µmol/kg, reaching upwards to about 50 m depth (Fig. 3b). As at 3°35’S the PCoastalC is located below 200 m depth and extends into to the deep ocean.

At 14°S the SLA shows a cyclonic eddy between 78 and 80°W and a strong anticyclonic eddy between 80 and 82°W (Fig. 1b). The latter eddy was formed in November 2008 near the Peruvian shelf and moved into this area from the east. The cyclonic eddy was formed in December 2008 near the shelf and moved westward following the anticyclonic eddy. The observed velocity field (Figure 3f) shows the anticyclonic eddy at 80 to 82°W as well as the cyclonic eddy between 78 and 80°W with velocities of about 30 cm/s. The cyclonic eddy has low oxygen water of less than 3 µmol/kg in its center (Fig. 3c) and indicates that these eddies are a potential source of low oxygen water from the coastal area to the open ocean OMZ. Both eddies cover the entire depth range to 700 m depth. The northward flow between 79°W and 81°W also includes the northward flowing HC/PCC. Near the shelf there is a strong signal of the PCCC with southward velocities of more than 10 cm/s also extending deep into the ocean. The PUC is not visible as a separate current band at 14°S, may have joined the PCCC as the latter shifted closer towards the shelf. The PCoastalC is only found close to the coast at 50 to 250 m depth. However, the short coastal sections at 12°S, at about 14°S, and at 16°S recorded in January 2009 resolve the PCoastalC near the shelf at 400 m depth (Fig. 1a), hence this northward flow is present at 12°S-16°S, although the different depth distributions indicate larger variability.

3.4. Float trajectories

The floats with a drift depth at 400 m were deployed in February 2009 at 10°S, 8°S, 6°S, 4°S and 2°S across the core of the open ocean South Pacific OMZ which expands vertically between the pycnocline and the intermediate water [*Fiedler and Talley*, 2006]. Typically the floats stay at the sea surface for about 0.5 days and at 400 m for 9.5 days for each cycle. To separate the surface and deep flow components the surface displacements are calculated between the first and the last float position at the sea surface received by ARGOS satellites during each cycle of the float. Displacements in 400 m depth are obtained between the last satellite contact at the surface before the float submerges and the first contact after the float surfaces [*Lebedev et al.*, 2007]. Estimates for the surface drift from February 2009 to August 2010 show that part of the westward displacement is due to the surface drift (Figure 4). The surface signal is strongest for the floats at 2°, 4° and 6°S, where the net surface westward displacement for the entire period is larger than 650 km.

Except for the float released at 8°S, the trajectories of floats for the 18-month period from February 2009 to August 2010 show a strong net westward movement. This general westward movement is surprising, since the ADCP section at 85°50’W as well as the model fields show large regions with eastward flow at 400 m depth. Also three of the five floats were deployed in regions with eastward flow at the time of deployment (Figure 2b).

The northernmost float (# 3901083) was deployed at 2°S (Fig. 4a) into the SICC (Fig. 2b). After the first cycle, the float left the SICC in a south-westward direction and followed the SEIC westward to 96°W in the latitude band between 2° - 3.5°S (Fig. 5). After the float drifted north-eastward from July to October 2009 it described a cyclonic loop, crossing the equator northward and moving westward along the equator within either the EIC or the NEIC (Fig. 5). As can be seen from figure 4, the net northward shift took place when the float was at the surface, while at 400 m depth the total net displacement is to the west.

At 4°S the float (# 3901081) was also deployed into the SEIC (Fig. 2b). The float generally follows the SEIC westward between 2° - 5°S until April 2010 (Fig. 5). At the surface this float moves slightly southward, in contrast with the northernmost float. At 400 m depth the float progresses mainly westward, except during December 2009 and January 2010, when the float moved straight to the north (Fig. 4b) leading to a mean northward component at 400 m depth. In April 2010 this float entered the SICC and moved eastward until July 2010. In July 2010 a southwestward component at the surface and at 400 m depth shifted the float back into the SEIC.

The float at 6°S (# 3901079) was deployed at the southern boundary of the SSCC, close to the SEC (Fig. 2b). Because of a strong southward component of the SSCC (Fig. 1) the float moved into the northern branch of the westward flowing SEC (Fig. 5). After the float had been displaced northward it re-entered the eastward flowing SSCC. The float crossed the SSCC northward and followed the SEIC westward between 3° and 7°S (Fig. 5). As for the float deployed at 4°S, the float deployed at 6°S has a net northward displacement at 400 m depth and a consistent westward flow at the surface (Fig. 4c).

The float at 8°S (# 3901077) was deployed into the SEC (Fig. 2b), however it moved south-eastward after the first cycle (Fig. 4). At 84.5°W the float turned north-westward and followed the SEC for about four months along the latitude band between 8° and 9°S from 85.5° to 90.5°W. After a cyclonic loop from October to December 2009, the float followed a strong southward current along 88.5°-90°W from 7.7°S to 10.9°S (Fig. 5). After January 2010 the float shifted east and in August 2010 it was further east than the deployment location in February 2009. For the 400 m depth component the float returned in August 2010 to almost the same location it had crossed 15 month earlier in May 2009 (Fig. 4c). The net westward displacement of this float is caused by the westward surface flow.

At 10°S the float (# 3901075) drifted south-eastward after deployment within the SECC (Fig. 1, 4e). After a northward displacement in April 2009, the float entered the westward flowing SEC in June (Fig. 5). The float follows the SEC for about five months within the latitude band 10° to 11°S (Fig. 4e, 5). The float, located at 91.5°W in November 2009, shows a meandering eastward drift, maybe within the SECC (Fig. 5), until April 2010. After April 2010 the float again moves westward with a strong westward displacement in June and July as in the year before.

At 400 m depth the three northernmost floats, deployed between 2° and 6°S, cover a net westward distance of 1200 to 1600 km and a meridional net distance of less than 270 km (Fig. 4a-c) within a time span between 520 and 522 days indicating a strong EIC, NEIC and SEIC in the latitude band between 2°N and 5°S. The westward current band in the equatorial region is likely intensified by the strong El Niño in 2009. The surface tracks also indicate a large net westward displacement. The two northernmost floats, deployed at 2° and 4°S (Fig. 4a, b), move about 1080 km northwestward and 835 km westward, respectively, within a time span of about 30 days and 29 days respectively, while the floats stayed at the sea surface. This corresponds to velocities of 42 cm s^{-1} and 33 cm s^{-1}. The strong meridional surface component of the northernmost float is notable, which covers a northward net distance of 330 km (Fig. 4a). By comparison the meridional net distance of the other floats at the surface is less than 100 km (Fig. 4b-d).

To compare with both models, TROPAC01 and SODA, we show the float tracks and the zonal velocity from the models at a depth of 400 m (Fig. 5a, b). As the floats were deployed at the beginning of an El Niño event in February 2009, we use the annual mean for both models from February 2002 to January 2003, which was also at the beginning of an El Niño.

The annual mean of zonal velocity in the TROPAC01 model indicates the strong westward currents EIC and NEIC between the equator and 2°N, representing the float tracks along the equator to west of 95°W (Fig. 5a). Two eastward current bands cross the region north of 5°S, probably associated with the SICC. The southern band is in the opposite direction of the predominantly westward float tracks in this region while the float returning east at about 108°W in May 2010 is consistent with the northern SICC band of TROPAC01. South of 5°S the zonal velocity field from the high resolution model describes the east- and westward current system very well in comparison with the float observations (Fig. 5a). The westward SEIC (4°S to 6.5°S) is in agreement with the westward float track at about 6°S. The eastward SSCC (6°S to 8°S) south of it is consistent with the eastward float drift along the latitude 7.5°S. The southernmost floats follow the westward SEC along 8°/9°S and 10°/11°S, respectively, in the time period from June/July to October, during which TROPAC01 has a westward current in the latitude band between 8°S to 11°S (Fig. 5a). In general TROPAC01 shows low annual mean zonal velocities of less than 2 cm/s in the region of the OMZ core.

SODA has a strong westward current band consisting of the NEIC, EIC and SEIC between 2°N to 5°S consistent with most of the float tracks in this area (Fig. 5b). Except east of 107°W the SODA model does not resolve the eastward SICC in the annual mean of the El-Niño-year 2002, which can be observed in ADCP sections (Fig. 2b). Just south of 5°S the SODA model shows the SSCC current band in most of the region. For the year 2002 the SODA model produces a strong SEC within 5°S to 7°S in a region where a float was drifting northwestward in 2009 (Fig. 5b). The SEC in SODA is located farther north than in TROPAC01 and the eastern part of the current band is twice as strong. This is caused by a stronger north-south shifting of the SEC throughout the year and the higher horizontal resolution of the TROPAC01 model. South to the SEC the SODA zonal velocity field is almost everywhere eastward between 9°S to 15°S, which is in the opposite direction of the two southernmost floats during the time between June to October (Fig. 4e). In general, both models represent the float tracks well. It is notable, that we use an annual mean for the model velocity fields at 400 m, therefore the model results do not resolve eddies or meandering tracks, which can be observed in the float velocity.

Based on the mean oxygen distribution at 400 m depth the center of the OMZ is located at about 8°S near 85°W and off the coast of Peru with mean oxygen values below 10 µmol/kg (Fig. 6). The low oxygen layer stretches west-north-westward and increases, with a mean value of about 15 µmol/kg at 6°S, 110°W. From the float tracks it is clear that the floats stayed much longer in the center of the OMZ while at the northern rim the westward progression is much faster. As the main westward movement for the two southern floats mainly takes place during the time the floats are at the surface transmitting their data, the westward movement at depth is greatly overestimated. In the center of the OMZ at about 8°S the net westward surface displacement accounts for 150% of the overall net westward displacement. The float tracks show that despite the relatively high velocities observed in the ADCP data at 85°50'W and 400 m depth the water stays longer in the region with less exchange with water with higher oxygen content. In addition the reversal of the flow direction at 400 m depth keeps the floats and the water in the center of the OMZ.

Oxygen concentration from the float deployed at 4°S shows a predominant vertical increase in oxygen > 40 µmol/kg as it propagates, while the minimum in the core of the OMZ stays at a relatively low value of less than 4 µmol/kg (Figure 7b). The strongest vertical increase in oxygen took place in January and February 2010 at the time when the float shifted north by about 200 km. Although the float changed from westward to eastward direction in April 2010 (Fig. 7a) no oxygen decrease is observed, except for a small decrease near 200 m depth showing that there are low zonal oxygen gradients in the SICC. After the end of 2009 the depth of the lowest oxygen values shifted upwards from about 400 m depth to 300 m in August 2010. At 400 m depth oxygen increased to more than 20 μmol/kg in May 2010, similar to what is expected on the westward increase of oxygen at 400 m depth (Figure 6).

4. Summary and Conclusions

The circulation in the eastern tropical South Pacific oxygen minimum zone is investigated using ADCP measurements, float tracks and model fields (TROPAC01 and SODA). The focus of this study was to better understand the weak flow field in the OMZ and the spreading pathways from the different methods. The eastern tropical South Pacific is a region with weak currents, so that short term-variability like wind events and eddies play an important role in this region. Nevertheless, information about the mean flow field is gained. Near the core of the OMZ at 400 m depth the currents in the center of the OMZ are relatively stagnant and the floats stayed much longer in the region than the floats at the northern side of the OMZ, which travel fast westward within the equatorial current system. Even floats deployed in a region of eastward flow moved westward over the 18 months, as the floats shifted between the eastward and westward current bands. The floats at 8° and 10°S reversed in zonal direction which supports the notion that they stay in the region. Considering only the 400 m flow component of the float deployed at 8°S it returned to a location it crossed in May 2009 in August 2010, 15 months later. *Wyrtki* [1967] concluded that a sluggish circulation led to long residence time in the OMZ of this region. The floats had been deployed in February 2009 at the beginning of an El Niño year, and the flow paths were compared with the mean model fields of an earlier El Niño year, as the recent months are not yet available from the model output. Despite the mean model flow fields and the different year used, there is general agreement between the model results and the observed float flow paths.

Most current bands identified in the upper ocean [e.g. *Kessler*, 2006] were also observed in the OMZ layer especially south of about 4°S (Fig. 2, 3), although they are weaker and more variable than in the upper ocean. The schematic flow field for the mid-depth OMZ layer at about 400 m depth (Fig. 8) combines the results described here with results that have been previously reported for the equatorial currents near the equator [*Stramma et al.,* 2010; *Rowe et al.,* 2000] and the mesoscale eddy-field [*Chaigneau et al.,* 2008]. The lowest DO values at mid-depth between 6°S and 10°S are located between the eastward flowing SSCC to the north and the northwestward flowing northern branch of the SEC to the south. Therefore the region south of the OMZ is covered by the northern part of the subtropical gyre, while to the north the region is governed by the complicated zonal equatorial flow field. The eastern Pacific between 8°S and 10°S is also a region with high eddy occurrence. The eddies move westward from the formation region near the shelf and carry water with low DO from the shelf region westward with velocities of 3 to 6 cm/s [*Chaigneau et al.,* 2008]. A cyclonic eddy with low oxygen in its core clearly demonstrates the contribution of low oxygen water to the OMZ. Hence the westward extending core of the OMZ at 6 to 10°S seems to be maintained by stagnant flow supplied with additional low DO water from the near shelf region by westward propagating eddies. The southern area with high frequency of eddy occurrence at 16°S to 18°S feeds low DO water into the HC/PCC to the SEC transition area leading to low DO values at the southeastern part of the OMZ. The PUC was observed only above 400 m (Fig. 3d-f) hence is not shown in Figure 8. For the upper layers of the OMZ the PUC is classically associated with the OMZ [e.g. *Strub et al.,* 1998], and our velocity observations support the notion, that the PUC is an important component of maintaining the OMZ in the upper OMZ. Given that direct measurements were made at the beginning of an El Niño year, the mean flow field might be slightly biased compared to non El Niño years, nevertheless we expect that the mean flow field of the mid-depth tropical southeast Pacific at 400 m depth (Fig. 8) is well resolved and that the resulting schematic mean flow field is accurate.

Appendix A. List of current band acronyms

EIC	Equatorial Intermediate Current
EUC	Equatorial Undercurrent
HC/PCC	Humboldt Current/Peru-Chile Current
NECC	North Equatorial Countercurrent
NEIC	North Equatorial Intermediate Current
NICC	North Intermediate Countercurrent
NSCC	Northern Subsurface Countercurrent
PCCC	Peru-Chile Countercurrent
PCoastalC	Peru Coastal Current
PUC	Poleward Undercurrent
SEC	South Equatorial Current
SEC(n)	Northern equatorial branch of the SEC
SEC(s)	Southern equatorial branch of the SEC
SECC	South Equatorial Countercurrent
SEIC	South Equatorial Intermediate Current
SICC	South Intermediate Countercurrent
SSCC	Southern Subsurface Countercurrent

Appendix B. List of floats deployed at a parking depth of 400 m

WMO number	Deployment time		Deployment position	
	date	time (UTC)	latitude	longitude
# 3901075	02.02.09	9:23	9°59.99’ S	85°50.00’ W
# 3901077	03.02.09	5:31	8° 0.01’ S	85°49.99’ W
# 3901079	09.02.09	21:25	6° 0.01’ S	85°50.00’ W
# 3901081	10.02.09	19:35	4° 0.10’ S	85°50.03’ W
# 3901083	11.02.09	14:44	2° 0.16’ S	85°50.02’ W

Acknowledgments. Financial support was received through the IFM-GEOMAR. This work is a contribution of Sonderforschungsbereich 754 “Climate – biogeochemistry interactions in the tropical ocean” (www.sfb754.de) which is supported by the Deutsche Forschungsgemeinschaft (RC, LS and JK TP-A5, FUS TP-A2). BSG is grateful for support from NOAA (grant NA06OAR4310146) and NSF (grant OCE-0351804). AF received funding through Deutsches Bundesministerium für Bildung und Forschung (BMBF) as part of the Verbundvorhaben Nordatlantik (03F0443B). The float data were collected and made freely available by the International Argo Project and the national programs that contribute to it (http://www.argo.ucsd.edu, http://argo.jcommops.org). Argo is a pilot program of the Global Ocean Observing System. The altimeter products were produced by Ssalto/Duacs and distributed by Aviso with support from Cnes. TROPAC01 was intergrated at the North-German Supercomputing Alliance (HLRN).

References

Ascani, F., E. Firing, P. Dutrieux, J. P. McCreary, and A. Ishida (2010), Deep equatorial ocean circulation induced by a forced-dissipated Yanai beam, *J. Phys., Oceanogr., 40*, 1118-1142.

Barnier, B, L. Brodeau, J. Le Sommer, J.-M. Molines, T. Penduff, S. Theetten, A.-M. Treguier, G. Madec, A. Biastoch, C. Böning, J. Dengg, S. Gulev, B.R. Bourdallé, J. Chanut, G. Garric, S. Alderson, A. Coward, B. de Cuevas, A. New, K. Haines, G. Smith, S. Drijfhout, W. Hazeleger, C. Severijns, and P Myers (2007), Eddy-permitting Ocean Cirsulation Hindcasts of past Decades, *CLIVAR Exchange*, *12*(3), 8-10.

Boyer, T.P., J. I. Antonov, O. K. Baranova, H. E. Garcia, D. R. Johnson, R. A. Locarnini, A. V. Mishonov, D. Seidov, I. V. Smolyar, and M. M. Zweng (2009), World Ocean Database 2009, Chapter 1: Introduction, NOAA Atlas NESDIS 66, Ed. S. Levitus, U.S. Gov. Printing Office, Wash., D.C. , 216 pp., DVD.

Boyer, T.P., J.I. Antonov, H. Garcia, D.R. Johnson, R.A. Locarnini, A.V. Mishonov, M.T. Pitcher, O.K. Baranova, and I. Smolyar (2006), World Ocean Database 2005, Chapter 1: Introduction, NOAA Atlas NESDIS 60, Ed. S. Levitus, U.S. Government Printing Office, Washington D.C., 182 pp., DVD.

Brandt, P., V. Hormann, A. Körtzinger, M. Visbeck, G. Krahmann, L. Stramma, R. Lumpkin, and C. Schmid (2010), Changes in the ventilation of the oxygen minimum zone of the tropical North Atlantic, *J. Phys. Oceanogr.,40*, 1784-1801.

Carton, J.A., G. Cherupin, X. Cao, and B.S. Giese (2000), A simple ocean data assimilation analysis of the global upper ocean 1950-95. Part I: methodology, J.

Phys., Oceanogr., 30, 294-309.

Carton, J.A., and B.S. Giese (2008), A reanalysis of ocean climate using SODA, *Mon. Wea. Rev., 136,* 2999-3017.

Chaigneau, A., A. Gizolme, and C. Grados (2008), Mesoscale eddies off Peru in altimeter records: Identification algorithms and eddy spatio-temporal patterns, *Prog. Oceanogr., 79*, 106-119.

Davis, R.E., (2005), Intermediate-depth circulation of the Indian and South Pacific oceans measured by autonomous floats, *J. Phys. Oceanogr., 35,* 683-707.

Debreu, L., C. Vouland and E. Blayo (2008), AGRIF: Adaptive grid refinement in Fortran, *Computers and Geoscience, 34,* 8-13, doi:10.1016/j.cageo.2007.01.009.

Dewitte, B., M. Ramos, V. Echevin, O. Pizarro, and Y. du Penhoat (2008), Vertical structure variability in a seasonal simulation of a medium-resolution regional model of the Eastern South Pacific, *Prog. Oceanogr., 79*, 120-137.

Eden, C., and A. Timmermann (2004), The influence of the Galapagos Islands on tropical temperatures, currents and the generation of tropical instability waves, *Geophys. Res. Lett., 31,* L15308, doi:10.1029/2004GL020060.

Fiedler, P.C., and L.D. Talley (2006), Hydrography of the eastern tropical Pacific: A review, *Prog. Oceanogr., 69,* 143–180.

Fine, R.A., K.A. Maillet, K.F. Sullivan, and D. Willey (2001), Circulation and ventilation flux of the Pacific Ocean, *J. Geophys. Res., 106*(C19), 22,159-22,178.

Firing, E., S. E. Wijffels, and P. Hacker (1998), Equatorial subthermocline currents across the Pacific, *J. Geophys. Res., 103*(C10), 21,413–21,423.

Giese, B.S., G. A. Chepurin, J. A. Carton, T. P. Boyer, and H. F. Seidel (2010): Impact of bathythermograph temperature bias models on an ocean reanalysis, J. Clim., doi:10.1175/2010JCLI3534.1.

Griffies, S. M., A. Biatoch, C. Böning, F. Bryan, G. Danabasoglu, E. P. Chassignet, M. H. England, R. Gerdes, H. Haak, R.W. Hallberg, W. Hazeleger, J. Jungclaus, W.G. Large, G. Madec, A. Pirani, B. L Samuels, M. Scheinert, A. Sen Gupta, C. A. Severijnsm H. L. Simmons, A.-M. Treguier, M. Wintin, S. Yeager, and J. Yin (2009), Coordinated Ocean-ice Reference Experiments (COREs), *Ocean Modelling*, *26*, 1-46, doi:10.1016/j.ocemod.2008.08.2007.

Johnson, G.C., B.M. Sloyan, W.S. Kessler, and K.E. McTaggart (2002), Direct measurements of upper ocean currents and water properties across the tropical Pacific during the 1990s, *Prog. Oceanogr.*, *52*, 31–61.

Karnauskas, K. B., R. Murtugudde, and A. J. Busalacchi (in press), Observing the Galapagos-EUC interaction: insights and challenges, *J. Phys. Oceanogr.*, doi: 10.1175/2010JPO4461.1.

Karstensen, J., L. Stramma, and M. Visbeck (2008), Oxygen minimum zones in the eastern tropical Atlantic and Pacific Oceans, *Prog. Oceanogr.*, *77*, 331–350.

Kessler, W.S., (2006), The circulation of the eastern tropical Pacific: A review, *Prog. in Oceanogr., 69*, 181–217.

Large, W. G., and S.G. Yeager (2009), The global climatology of an interannually varying air-sea flux data set, *Climate Dynamics*, *33* (2-3), 341-364, doi:10.1007/s00382-008-0441-3.

Lebedev, K. V., H. Yoshinari, N. A. Maximenko, and R. W. Hacker (2007), YoMaHa'07: Velocity data assessed from trajectories of Argo floats at parking level and at the sea surface, *IPRC Technical Note No.4(2)*, June 12, 2007, 16p.

Levitus, S., J.I. Antonov, T.P. Boyer, R.A. Locarnini, H. E. Garcia and A.V. Mishonov, H.E. Garcia, 2009: Global Ocean Heat Content 1955-2007 in light of recently revealed instrumentation problems. *Geophys. Res. Lett, 36*, doi: 10.1029/2008GL037155.

Luyten, J.R., J. Pedlosky, and H. Stommel (1983), The ventilated thermocline, *J. Phys. Oceanogr., 13*, 292–309.

Madec, G. (2008), NEMO ocean engine - version 3.1, *Note du Pôle de modélisation de l'Institut Pierre-Simon Laplace No 27*.

Montes, I., F. Colas, X. Capet, and W. Schneider (2010), On the pathways of the equatorial subsurface currents in the eastern equatorial Pacific and their contribution to the Peru-Chile Undercurrent, *J. Geophys. Res., 115*, C09003, doi:10.1029/2009JC005710.

Paulmier, A., and D. Ruiz-Pino (2009), Oxygen minimum zones (OMZs) in the modern ocean. *Prog. Oceanogr., 80*, 113–128.

Penven, P., V. Echevin, J. Pasapera, F. Colas, and J. Tam (2005), Average circulation, seasonal cycle, and mesoscale dynamics of the Peru Current system: A modeling approach, *J. Geophys. Res., 110,* C10021, doi:10.1029/2005JC002945.

Pizarro, O., G., Shaffer, B. Dewitte, and M. Ramos (2002), Dynamics of seasonal and interannual variability of the Peru-Chile Undercurrent, *Geophys. Res. Lett., 29,* 1581, 10.1029/2002GL014790.

Reid, J.L., (1986), On the total geostrophic circulation of the South Pacific Ocean: flow patterns, tracers and transports, *Prog. Oceanog.,* 16, 1-61.

Reid, J.L., (1997), On the total geostrophic circulation of the Pacific Ocean: flow patterns, tracers and transports, *Prog. Oceanog.*, 39, 263-352.

Rowe, G.D., E. Firing, and G.C. Johnson (2000), Pacific Equatorial Subsurface Countercurrent Velocity, Transport, and Potential Vorticity, *J. Phys. Oceanogr., 30,* 1172–1187.

Schott, F.A., J.P. McCreary and G.C. Johnson (2004), Shallow overturning circulation of the tropical-subtropical oceans, in *Earth's Climate: The Ocean Atmosphere Interaction,* edited by C. Wang, S.-P. Xie, and J.A. Carton, pp. 261–304, AGU, Washington, D.C.

Stramma, L., G.C. Johnson, J. Sprintall, and V. Mohrholz (2008), Expanding oxygen-minimum zones in the tropical oceans, *Science, 320*, 655–658.

Stramma, L., G.C. Johnson, E. Firing, and S. Schmidtko (2010), Eastern Pacific oxygen minimum zones: supply paths and multi-decadal changes, *J. Geophys. Res.*, 115, C09011, doi: 10.1029/2009JC005976..

Strub, P.T., J.M. Mesias, and C. James (1995), Altimeter observations of the Peru-Chile Countercurrent, *Geophys. Res. Let., 22,* 211-214.

Strub, P.T., J.M. Mesias, V. Montecino, J. Rutllant, and S. Salinas (1998), Coastal ocean circulation off western South America, in *The Sea,* vol. 11, edited by A. R. Robinson and K. H. Brink, pp. 273-314, John Wiley, Hoboken, N.J.

Tsimplis, M.N., S. Bacom, and H.L. Bryden (1998), The circulation of the subtropical South Pacific derived from hydrographic data, *J. Geophys. Res., 103*(C10), 21,443-21,468.

Tsuchiya, M., and L. D. Talley (1998), A Pacific hydrographic section at 88°W: Water-property distribution, *J. Geophys. Res., 103*(6), 12,899–12,918.

Wyrtki, K., (1967), Circulation and water masses in the eastern equatorial Pacific Ocean, *Int. J. Oceanol. & Limnol., 1*(2), 117-147.

Figure Caption

Figure 1. Horizontal distribution of a) ADCP velocity vectors at 400 m depth recorded between 5 January and 14 February 2009 with current bands indicated by arrows (see text in section 3.1 for details) and the mean climatological oxygen distribution at 400 m (in µmol/kg, with 5µmol/kg contour spacing, thin lines) from WOA05 [*Boyer et al.,* 2006] and b) altimeter derived sea level anomaly in cm on 4 February 2009 [http://www.aviso.oceanobs.com]. ADCP and CTD sections are shown as black lines. Arrows indicate the related flow direction.

Figure 2. Zonal oxygen in µmol/kg and velocity distribution (in cm s^{-1}; positive eastward) for a) oxygen distribution at 85°50’W in February 2009, b) ADCP measurements at 85°50’W in February 2009, c) velocity from TROPAC01 at 85°48’W in February 2002, and d) SODA model velocity distribution at 86°W in February 2002. The black circles at 400 m depth at 10°S, 8°S, 6°S, 4°S and 2°S are the deployment locations of the floats. See text of section 3.2 for indicated current bands.

Figure 3. Meridional oxygen in µmol/kg and velocity distribution (in cm s^{-1}; positive northward) for oxygen measurements at a) 3°35’S in early February 2009, b) 6°S in early February 2009, c) 14°S in late January 2009 and for ADCP measurements at d) 3°35’S in early February 2009, e) 6°S in early February 2009) and f) 14°S in late January 2009. See text of section 3.3 for indicated current bands.

Figure 4. Progressive spreading paths in km for the zonal and meridional spreading components between February 2009 and mid-August 2010 for the 5 floats with a parking depth at 400 m, separating the components at the surface (red, white) and at 400 m (blue, white). Even months are blue and red, odd months are white. Stars mark the beginning of year 2010. Zero is located at the deployment location at 85°50’W and a) 2°S, b) 4°S, c) 6°S, d) 8°S and e) 10°S, respectively. Note the different x-scales.

Figure 5. Zonal velocity distribution (in cm s^{-1}) at 400 m depth averaged from February 2002 to January 2003 for a) TROPAC01 and b) SODA. Float trajectories in 400 m depth for February 2009 to mid-August 2010 are also shown. Eastward velocity is plotted white and red, westward velocity is plotted grey and blue.

Figure 6. Mean climatological oxygen distribution in μmol/kg at 400 m from WOA05 [*Boyer et al*. 2006], velocities derived from float tracks for five 400-m floats (red arrows) between February 2009 and mid-August 2010 and the horizontal velocity vectors at 400 m depth from shipboard ADCP data in February 2009 (black arrows).

Figure 7. Time series from February 2009 to mid-August 2010 of the float (WMO #3901081) deployed at 4°S with 400 m parking depth for a) westward (gray) and eastward (white) displacements (in °) and b) oxygen profiles (in μmol/kg) of the upper 1500 m measured in 10-day intervals. The corresponding longitude is marked on top of b). The float is drifting westward with the SEIC until April 2010 when it entered the SICC flowing eastward (see figure 5).

Figure 8. Schematic mid-depth flow field at about 400 m depth. The mean climatological dissolved oxygen distribution at 400 m from WOA05 [*Boyer et al.*, 2006] is included (in µmol/kg, with 5 µmol/kg contour spacing, thin lines). Areas of high frequency of eddy occurrence [*Chaigneau et al.*, 2008] are marked by dashed lines.

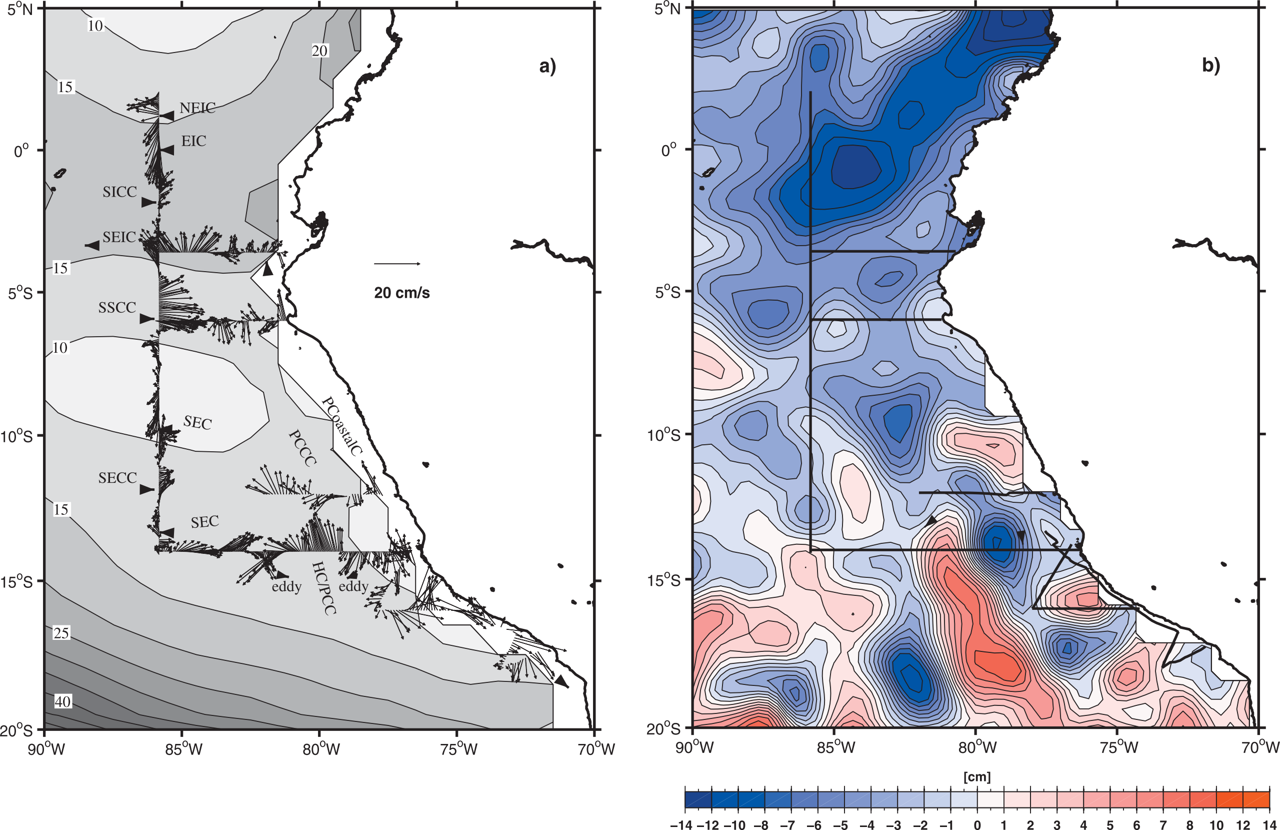
a)
b)
NEIC
EIC
SICC
SEIC
SSCC
SEC
SECC
SEC
PCCC
PCoastalC
HC/PCC
eddy
eddy
20 cm/s
10
15
20
15
10
15
25
40
5°N
0°
5°S
10°S
15°S
20°S
90°W
85°W
80°W
75°W
70°W
[cm]
−14
−12
−10
−8
−7
−6
−5
−4
−3
−2
−1
0
1
2
3
4
5
6
7
8
10
12
14

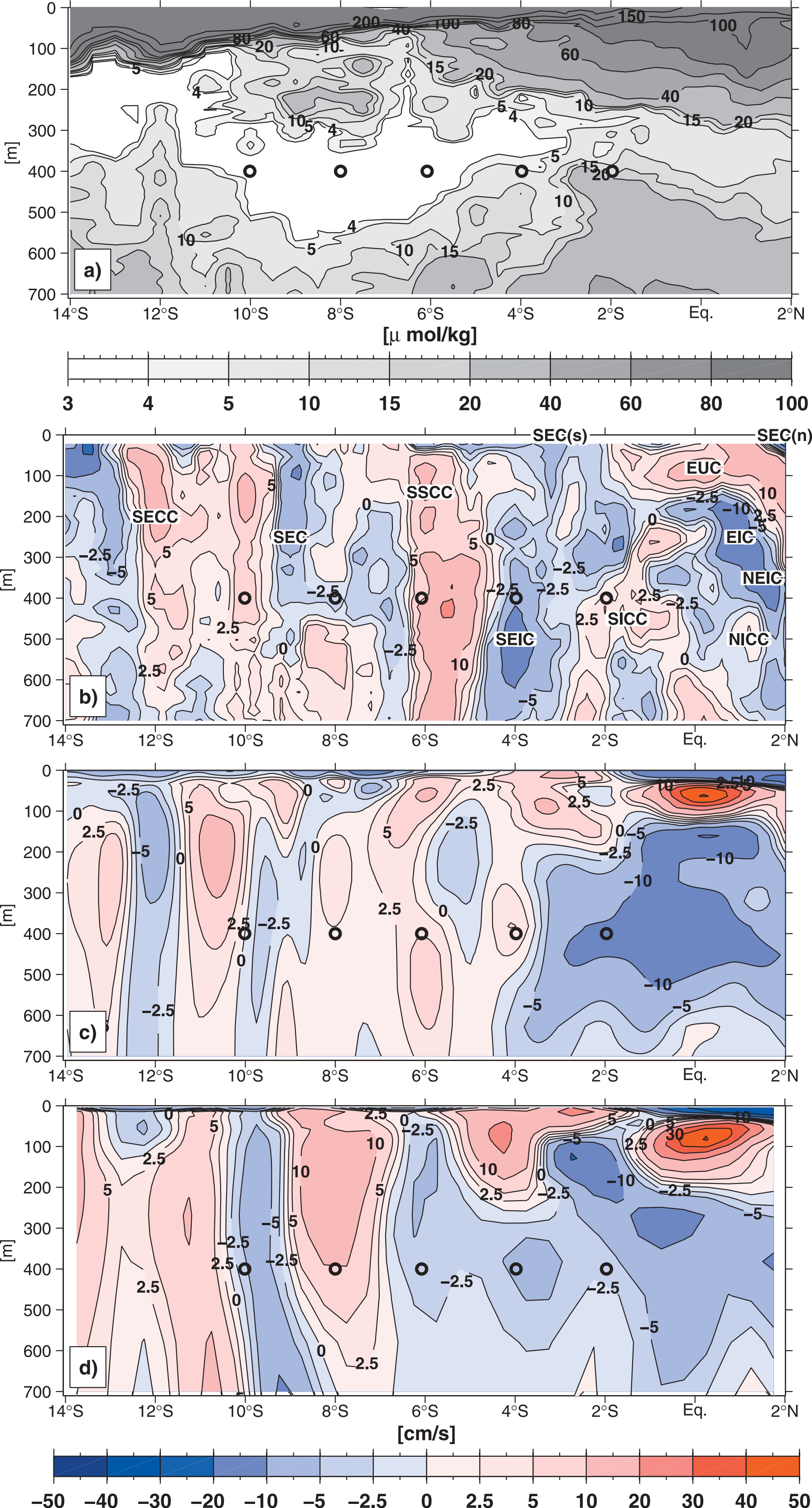
a)
b)
c)
d)
[m]
0
100
200
300
400
500
600
700
14°S
12°S
10°S
8°S
6°S
4°S
2°S
Eq.
2°N
[μ mol/kg]
3
4
5
10
15
20
40
60
80
100
SEC(s)
SEC(n)
EUC
SSCC
SECC
SEC
EIC
NEIC
SICC
SEIC
NICC
[cm/s]
−50
−40
−30
−20
−10
−5
−2.5
0
2.5
5
10
20
30
40
50

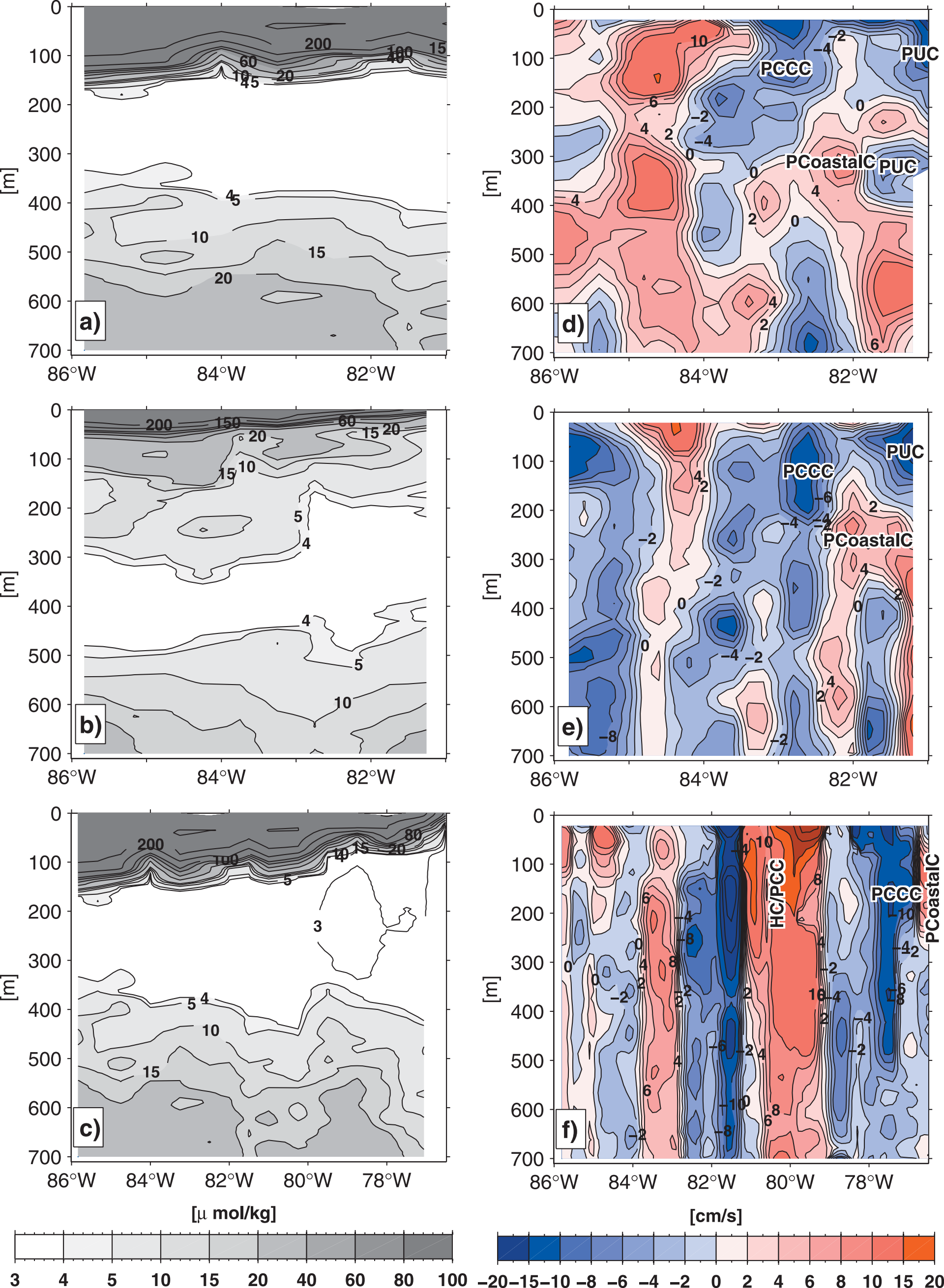
a)
b)
c)
d)
e)
f)
[m]
0
100
200
300
400
500
600
700
86°W
84°W
82°W
80°W
78°W
200
100
60
45
40
20
15
10
5
4
3
150
80
PCCC
PUC
PCoastalC
HC/PCC
[μ mol/kg]
[cm/s]
3 4 5 10 15 20 40 60 80 100
−20 −15 −10 −8 −6 −4 −2 0 2 4 6 8 10 15 20

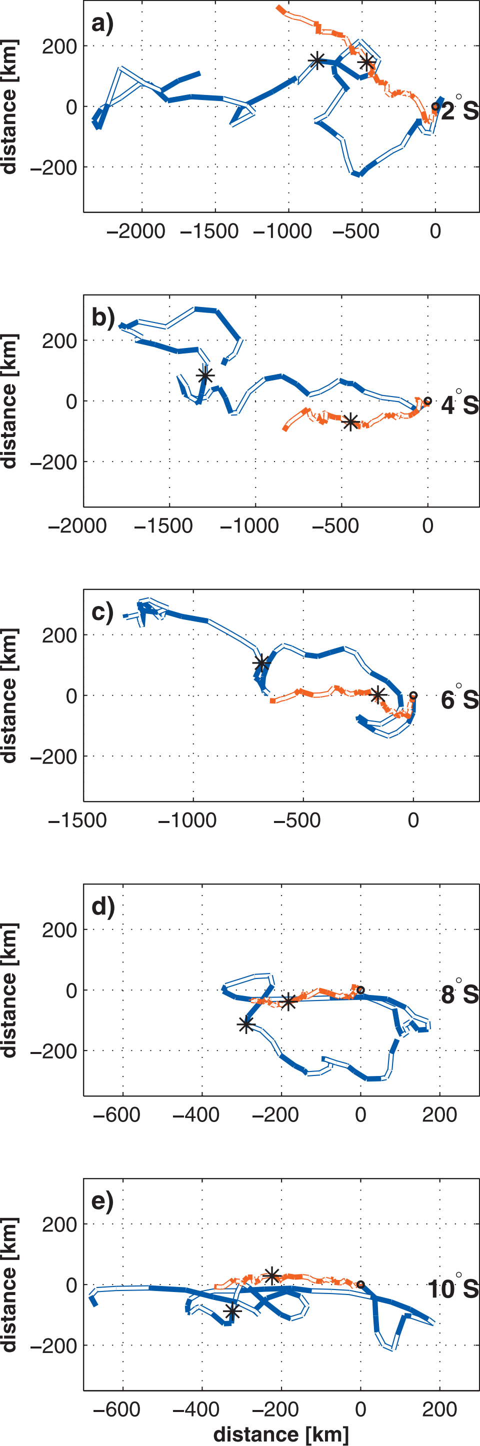
a)
2°S
b)
4°S
c)
6°S
d)
8°S
e)
10°S
distance [km]
distance [km]
200
0
−200
−2000
−1500
−1000
−500
0
−1500
−1000
−500
0
−600
−400
−200
0
200

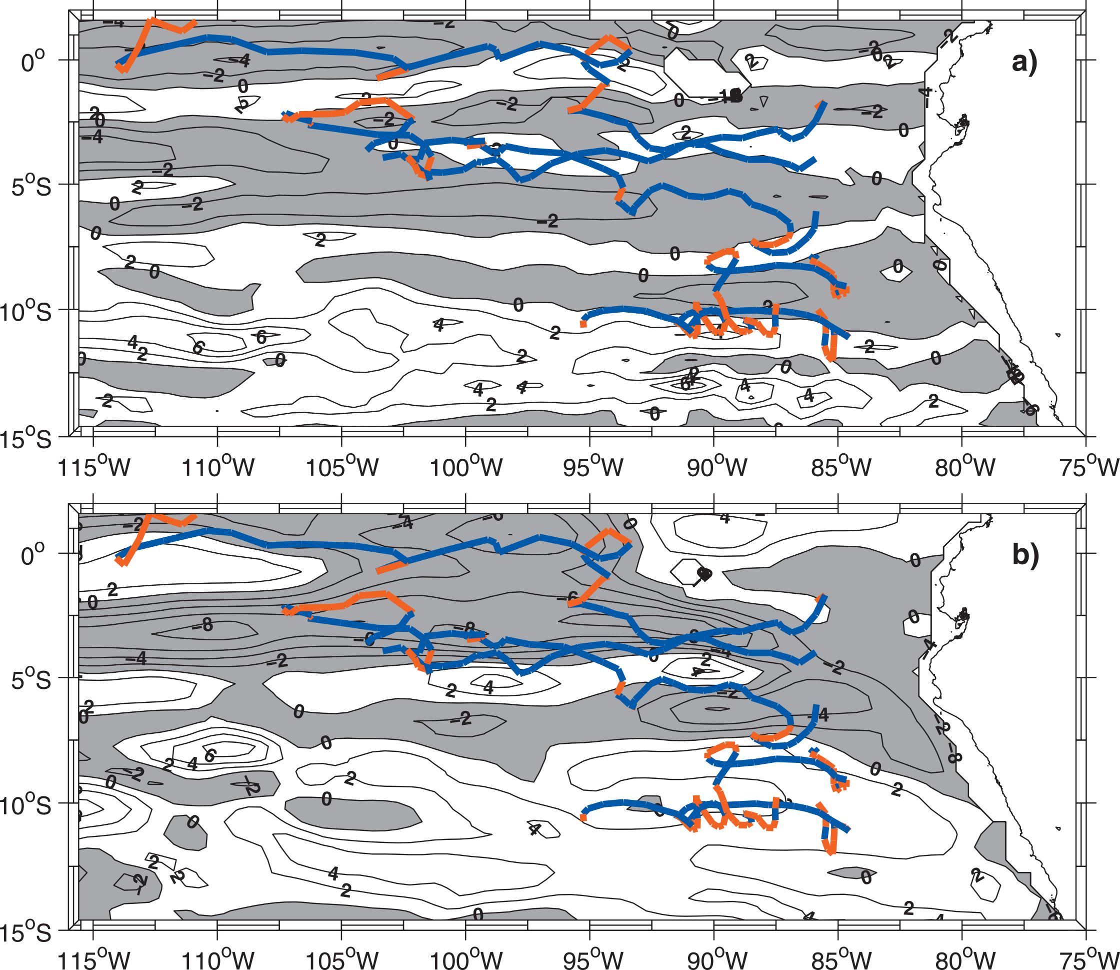
a)
b)
0°
5°S
10°S
15°S
115°W
110°W
105°W
100°W
95°W
90°W
85°W
80°W
75°W

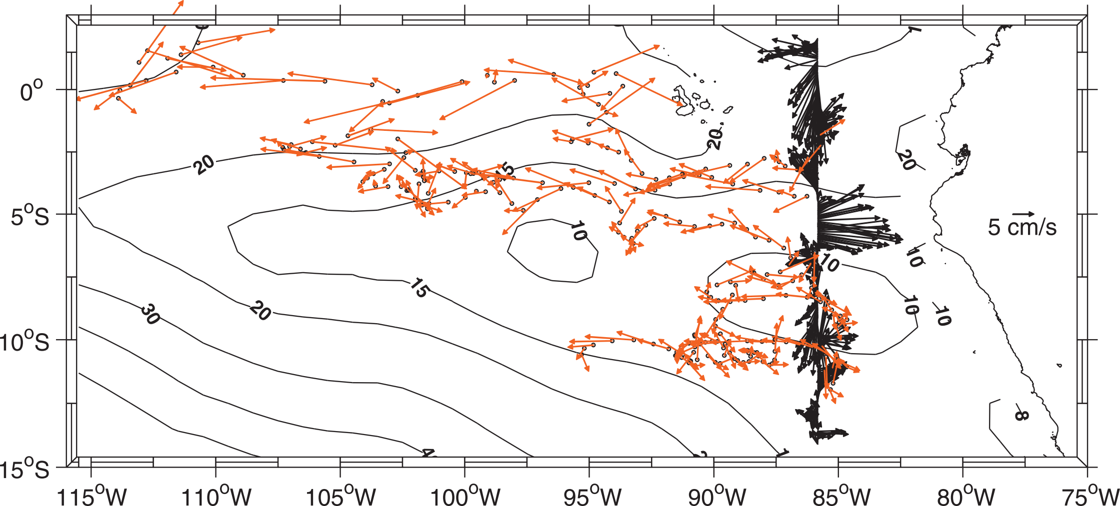
0°
5°S
10°S
15°S
115°W
110°W
105°W
100°W
95°W
90°W
85°W
80°W
75°W
5 cm/s
20
15
10
20
15
20
30
10
10
10
10
20
1
8

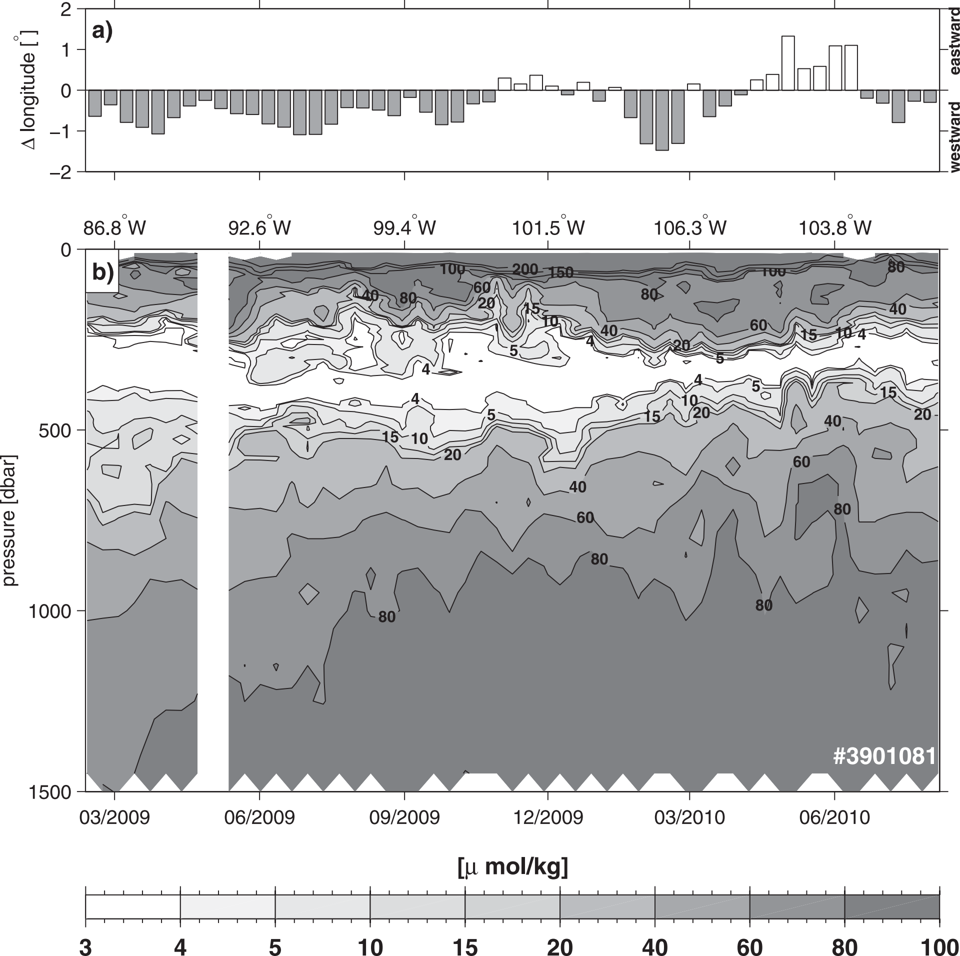
a)
Δ longitude [°]
eastward
westward
2
1
0
−1
−2
86.8°W
92.6°W
99.4°W
101.5°W
106.3°W
103.8°W
b)
pressure [dbar]
0
500
1000
1500
#3901081
03/2009
06/2009
09/2009
12/2009
03/2010
06/2010
[μ mol/kg]
3
4
5
10
15
20
40
60
80
100
200
150

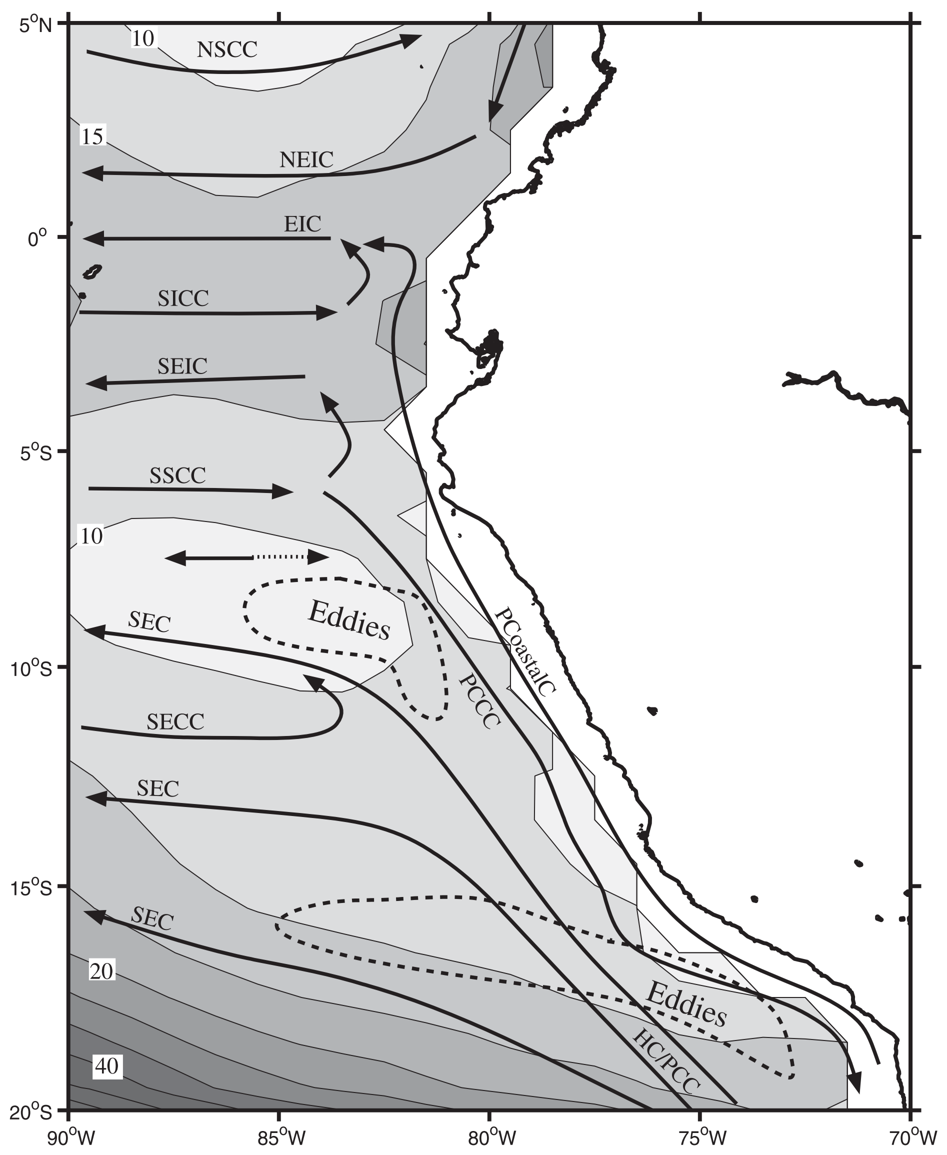
5°N
0°
5°S
10°S
15°S
20°S
90°W
85°W
80°W
75°W
70°W
10
NSCC
15
NEIC
EIC
SICC
SEIC
SSCC
10
Eddies
SEC
SECC
SEC
SEC
20
40
PCCC
PCoastalC
Eddies
HC/PCC